Optics Letters

Polarization-multiplexed multiplane display

Guanjun Tan, Tao Zhan, Yun-Han Lee, Jianghao Xiong, and Shin-Tson Wu*

CREOL, The College of Optics and Photonics, University of Central Florida, Orlando, Florida 32816, USA
*Corresponding author: swu@creol.ucf.edu

Received 22 August 2018; revised 11 October 2018; accepted 23 October 2018; posted 26 October 2018 (Doc. ID 342783); published 14 November 2018

We demonstrate a polarization-multiplexed multiplane display system for near-eye applications. A polarization-sensitive Pancharatnam–Berry phase lens is implemented to generate two focal depths simultaneously. A spatial polarization modulator is utilized to direct the two images to designated focal planes. Based on this design, a dual-focal-plane display system is constructed without space- or time-multiplexing operations, to suppress the vergence-accommodation conflict successfully. © 2018 Optical Society of America

https://doi.org/10.1364/OL.43.005651

Head-mounted displays (HMDs) are emerging and enabling novel applications in entertainment, education, and medical surgeries, just to name a few. In most of the current HMDs, stereoscopic display based on binocular disparity is usually adopted to create depth perception [1,2]. Two different images are separately sent to the left and right eyes to generate the illusion of depth. However, stereoscopic 3D perception results in the well-known vergence-accommodation conflict (VAC), which remains one of major challenges for HMDs [3]. Such a mismatch between vergence and accommodation distances is the main cause of visual discomfort and fatigue [4,5] when wearing such a headset.

Several approaches have been developed to overcome the VAC issue [6–17]. Generally, these solutions can be divided into two categories [3]: static (space-multiplexed) and dynamic (time-multiplexed) approaches. The static category typically includes stacked panels [6–8], integral displays [9], and scanned fiber arrays [10]. Major challenges of static approaches are the difficulties to stack multiple focal planes in a compact way, and the loss of display resolution and contrast [3]. Time-multiplexed methods do not necessarily involve multiple display screens, which enables more compact designs [3]. Dynamic approaches change the image depths time-sequentially to provide the correct focus cues [3]. However, some tunable optical elements, such as a deformable mirror [11], tunable lens [12–16], or switchable diffuser [17], are needed in a dynamic design. Therefore, time-multiplexing methods require a high display frame rate and fast response time of tunable optics, because the required refresh rate increases with the number of focal depths.

In this Letter, we report a multiplane display using polarization-multiplexing operation, instead of space or time multiplexing. A polarization-sensitive Pancharatnam–Berry phase lens (PBL) and a liquid crystal (LC) spatial polarization modulator (SPM) are used to simultaneously create two independent focal planes. This method enables the generation of two image planes without the need for temporal multiplexing or switchable lenses. Thus, the proposed design can effectively reduce the frame rate by one half.

In a Pancharatnam–Berry phase optical element, a half-wave ($\lambda/2$) plate is spatially patterned with varying crystal axis direction [15,18–20]. Its phase modulation is directly related to the crystal axis orientation, namely LC azimuthal angle $\phi(x,y)$. The working principle can be explained by Jones matrices. First, the polarization state of a circularly polarized light can be written as

$$J_{\pm} = \frac{1}{\sqrt{2}}\begin{bmatrix} 1 \\ \pm i \end{bmatrix}, \tag{1}$$

where J_+ and J_- stand for the left- and right-handed circularly polarized light (LCP and RCP), respectively. After the circularly polarized light passes through a $\lambda/2$ plate, the output can be calculated by [15,16]

$$J'_{\pm} = R(-\varphi)\cdot W(\pi)\cdot R(\varphi)\cdot\frac{1}{\sqrt{2}}\begin{bmatrix} 1 \\ \pm i \end{bmatrix} = e^{\pm i2\varphi}\frac{1}{\sqrt{2}}\begin{bmatrix} 1 \\ \mp i \end{bmatrix}, \tag{2}$$

where R presents the rotation operation matrix and W is the phase retardation matrix. From Eq. (2), the handedness of outgoing circularly polarized light is flipped. In addition, the $\lambda/2$ plate also introduces a phase delay of $\pm 2\phi(x,y)$ to LCP and RCP, respectively. In a PBL, the spatial distribution of the LC director azimuthal angle $\phi(x,y)$ follows paraboloid function, as Fig. 1(a) illustrates. Thus, for a circularly polarized light, a paraboloid phase distribution can be constructed. Please note that the phase profiles of LCP and RCP lights have opposite signs [Fig. 1(b)]. Therefore, if the PBL is designed to work as a diverging lens for LCP, then it is a converging lens for RCP, as Fig. 2 depicts. Basically, PBL is a polarization-sensitive bifocal lens with high polarization selectivity.

According to Fig. 2, a PBL can offer two focal planes simultaneously, depending on the incident polarization. However, achieving multiple image planes is just the first step to realize a multiplane display. We need to assign correct images to these

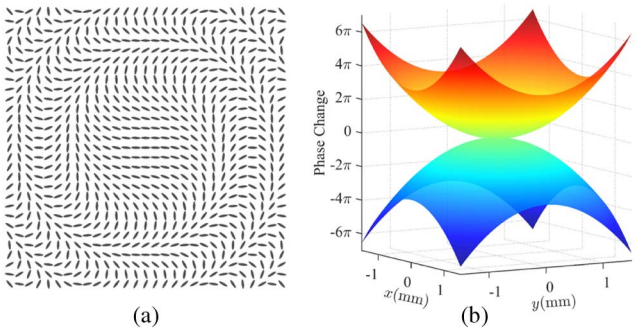

Fig. 1. (a) Top view of the LC director distribution and (b) phase change profile of a PBL with ±0.8 D optical power for RCP and LCP.

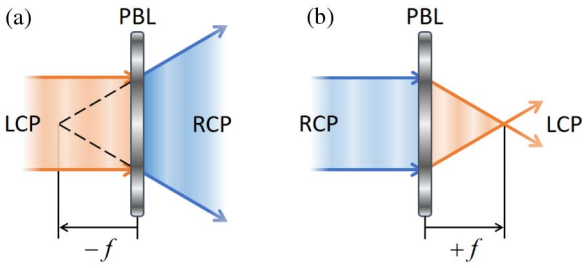

Fig. 2. (a) The PBL serves as a diverging lens for LCP light, and (b) the PBL serves as a converging lens for RCP light.

focal planes. Based on the PBL's excellent polarization selectivity, we can adopt the polarization-multiplexing operation to send independent images to these focal planes. LCP and RCP are a set of basis for optical polarization state space. For a polarized light, it can be represented as a superposition of LCP and RCP waves, and its LCP and RCP components can be independently sent to the PBL's two focal planes, respectively. Thus, by modulating the incident light polarization, we can easily control the ratio of LCP and RCP, and generate independent images for two focal planes.

Figure 3 depicts the device configuration of our proposed polarization-multiplexed multiplane display. The display panel in Fig. 3 can be a liquid crystal display (LCD) or an organic light-emitting diode display with a circular polarizer (CP), which usually consists of a linear polarizer and a $\lambda/4$ plate. Without losing generality, we can assume the display panel

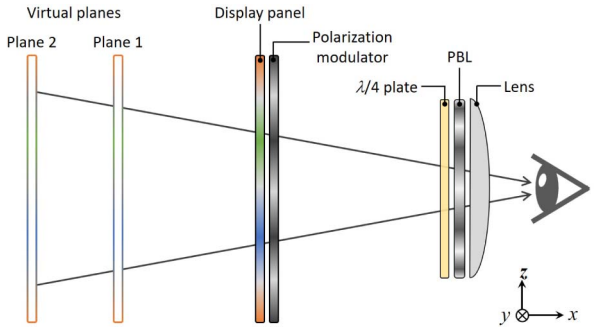

Fig. 3. Experimental setup of the proposed polarization-multiplexed multiplane display system.

emits a linearly polarized light along z axis (0°). Then a pixelated SPM is closely integrated and aligned to the display panel. The SPM in Fig. 3 is designed to obtain full-range modulation between two orthogonal polarization states, namely 0° and 90° in our system. The required polarization modulation is not just to switch between two states; we need continuous modulation to get intermediate states. With a broadband $\lambda/4$ plate oriented at 45°, these two orthogonal linear polarizations would be converted to RCP and LCP waves, respectively. Since our SPM can continuously modulate the polarization state, the relative ratio of RCP and LCP components can be tuned. With the help of a polarization-sensitive PBL, its RCP and LCP components will be sent to two virtual planes simultaneously, as Fig. 3 shows. In brief, the PBL simultaneously creates two focal depths, and the SPM directs the images to these two focal planes.

In Fig. 3, the display panel and polarization modulator jointly determine the displayed images of two virtual planes. How to input correct information data needs to be carefully considered as well. Let us assume that the target light intensity distributions in plane 1 and plane 2 are denoted as I_1 and I_2. The display panel in Fig. 3 needs to provide total light intensity I_{DP} as

$$I_{\mathrm{DP}} = I_1 + I_2. \tag{3}$$

Then the SPM is used to separate the two focal plane images. After SPM modulation, the light polarization may be modulated to 0°, 90° or any intermediate polarization state. The proportions of 0° and 90° polarization components to the total intensity should be

$$t_{0^\circ} = I_1/(I_1 + I_2),$$
$$t_{90^\circ} = I_2/(I_1 + I_2). \tag{4}$$

From Eq. (4), t_{0° and t_{90° can vary from 0 to 1. Thus, a full-range SPM is required. Please note that t_{0° and t_{90° are also spatially variable. After the $\lambda/4$ plate and PBL, I_1 and I_2 can be successively assigned to virtual planes 1 and 2, as Fig. 3 depicts.

In the experiment, we used a 4.7 inch 60 Hz LCD (iPhone 7, with resolution 1334 × 750) as the display panel. To prepare a SPM, we removed the polarizers of a commercial twisted nematic (TN) LCD panel (5.0 in., 60 Hz, 800 × 480) and used it as a SPM. The two reasons we chose TN LCD are 1) it can easily offer a full-range modulation between two orthogonal polarizations and 2) it is a broadband device with less wavelength dependency [21]. We then fabricated a 2.5 in. PBL with optical power ±0.8 D by interference exposure [15,22]. A glass substrate was first cleaned and spin-coated with a thin photo-alignment layer. A Mach–Zehnder interferometer with $\lambda = 442$ nm (He–Cd laser) was set up for exposure, whose two arms had opposite circular polarizations. A convex lens was positioned in one arm to obtain the desired interference pattern. After interference exposure, a UV-curable diluted LC monomer (RM257) was coated on the exposed substrate surface, which was then cured by a UV light to form a thin cross-linked LC polymer layer. The LC birefringence (Δn) and thickness (d) were carefully tuned to match the half-wave requirement for $\lambda = 550$ nm. More detailed fabrication procedures of the PBL can be found in [15,22]. Please note that the depth difference can be easily tuned by changing the optical setup of interference exposure. Moreover, in our system [Fig. 3], a positive lens with optical power 10 D was applied

to provide a biased focusing power. Thus, the accommodation depths of two focal images are 0.1 D and 1.7 D, respectively. The horizontal field of view of the experimental demonstration is close to ±35°.

Before constructing a multiplane display, we need to examine the display reproduction capability for the two focal planes. Based on Eqs. (3) and (4), we calculated I_{DP}, $t_{0°}$, and $t_{90°}$ for two target images with letter "A" and "B." The RGB channels in the full-color images were separately processed. Gamma 2.2 correction in the TN panel was taken into consideration as well. Then we loaded the intensity I_{DP} to the display panel and polarization modulation $t_{0°}$ and $t_{90°}$ to SPM. To examine the cross talk between two focal plane images, we inserted right-handed and left-handed CPs successively just after the $\lambda/4$ plate. A Canon EOS T5i camera was used to take photographs. Figure 4 shows that our system can simultaneously reproduce two independent images: letter "A" in RCP [Fig. 4(e)] and "B" in LCP [Fig. 4(f)]. While one may notice that there still exists small cross talk in Figs. 4(e) and 4(f), detailed measurements indicate that the cross talk between these two orthogonal polarizations is 0.27%, 0.42%, and 4.83% for $\lambda = 457$ nm, 514 nm, and 633 nm, respectively. This cross talk comes from the commercial TN panel, since it is optimized for display at $\lambda \approx 550$ nm, instead of polarization modulation.

With the help of the PBL, these two images with orthogonal polarizations should be sent to different focal depths. Letters "A" and "B" exist simultaneously while they are located at different depths [Fig. 5]. With the camera focusing at front virtual plane 1 [Fig. 5(a)], letter "A" was on focus with sharp edges, while letter "B" was blurred. When focusing at the rear plane, "A" became blurry.

To create correct 3D perception, the display images on two focal planes should be designed and optimized. Several different image-rendering methods can be applied on our system to generate 3D perception [8,16,23,24]. Here we adopted an additive factorization method to generate all the 2D images for corresponding image depths [8,16]. Since virtual planes 1 and 2 exist simultaneously as Fig. 6 depicts, total light intensity I_{total} along a specific direction can be directly calculated by

$$I_{total} = I_{1i} + I_{2j}, \tag{5}$$

where I_{1i} and I_{2j} represent the intensity of specific pixels along a specific direction from first and second virtual planes. After optimization, these two images can be generated. In our system with two virtual planes, we rendered two images for the 16 × 16 mm eye-box size with 5 × 5 viewing points. The rendered images are shown in Fig. 7.

With the rendered images obtained [Fig. 7], we calculated the intensity information I_{DP} and polarization modulation $t_{0°}$ and $t_{90°}$. Experimental results are shown in Figs. 8 and 9. Two cubes are located at different spatial positions: the pink–yellow cube at the right side with a near distance and the blue–green one at the left side with a far distance. The blue–green

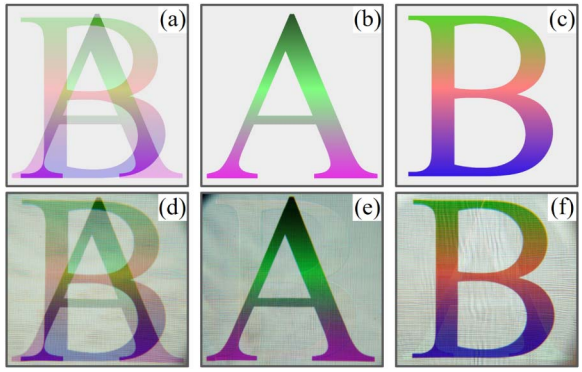

Fig. 4. Target images: (a) without CP, (b) with right-handed CP, and (c) with left-handed CP. Measured results: (d) without CP, (e) with right-handed CP, and (f) with left-handed CP.

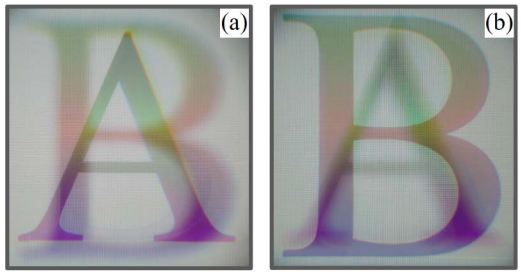

Fig. 5. Photographs captured with a camera focusing at (a) virtual plane 1 and (b) virtual plane 2.

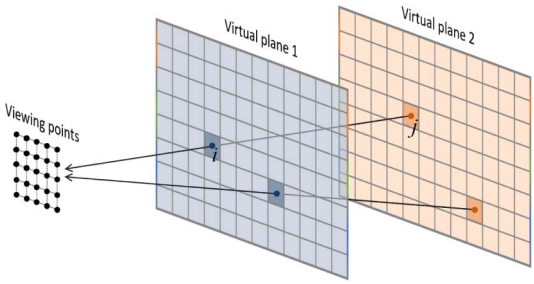

Fig. 6. Schematic diagram of the rendering method for two virtual planes.

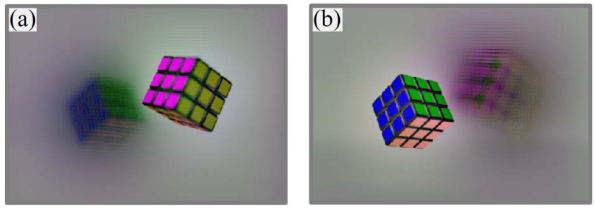

Fig. 7. Rendered images to be displayed in (a) virtual plane 1 and (b) virtual plane 2.

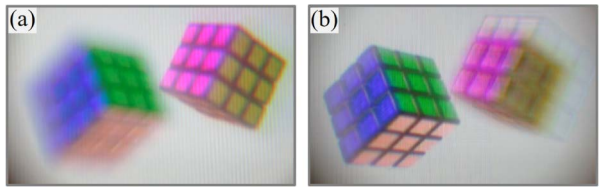

Fig. 8. Photographs captured with a camera focusing at the (a) front object and (b) rear object.

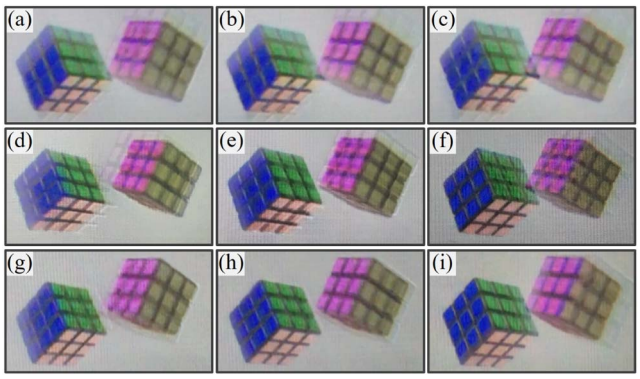

Fig. 9. Experimental photographs of the multiplane display at different viewing positions: (a) upper left, (b) upper, (c) upper right, (d) left, (e) central, (f) right, (g) lower left, (h) lower, and (i) lower right.

cube was blurry when focusing at the front plane [Fig. 8(a)], while the pink–yellow cube became blurry when focusing at the rear plane [Fig. 8(b)]. Figure 9 shows the photographs at different viewing positions. An obvious 3D parallax effect is clearly illustrated in Fig. 9. From different viewing points, we can see slightly different images. For instance, from left [Fig. 9(d)] to right [Fig. 9(f)], two cubes get closer and closer. Especially, at the right viewing points [Figs. 9(c), 9(f) and 9(i)], the front pink–yellow cube blocks a portion of the rear blue–green cube. Figures 8 and 9 demonstrate that our system can successfully realize a multiplane display with correct 3D reproduction capability. Since there are only two image planes in this proof-of-concept experiment, the occlusion issue is not well addressed [Figs. 9(c) and 9(f)], in which more image planes are eventually needed.

From Figs. 8 and 9, there remain noticeable ghost images, which could originate from the TN panel's polarization cross talk [Fig. 4] and the wavelength-dependent efficiency of the PBL. Normally, such a commercial TN panel is optimized for display applications at $\lambda \approx 550$ nm. Thus, for the blue and red wavelengths, such a TN LCD deviates slightly from an ideal polarization rotator, which leads to the observed cross talk between two focal image planes. One way to mitigate this issue is to increase the $d\Delta n$ value of the TN LCD. To address the wavelength-dependency of the PBL, a dual-twist structure [25,26] can be adopted to effectively improve the efficiency to >95% within the whole visible range [15,26].

As for virtual reality displays, a 6 K × 6 K resolution is desirable to minimize the screen-door effect [27]. In our design, the SPM is used mainly to provide depth information. Thus, it is not required for the SPM to match the resolution of the display panel. A relatively lower resolution of the SPM helps to reduce the possible Moiré effect when two panels are aligned together, and to improve the optical efficiency.

In our demonstration, we use one PBL to achieve two focal planes. To further improve the quality and functionality, the number of image planes, spacing between adjacent planes, and image rendering algorithm, all need to be taken into consideration [28–30]. According to Ref. [29], the spacing between two adjacent planes should be ~0.6 D, and five to six image planes are eventually needed. The proposed polarization-multiplexed approach can also be integrated with a space- or time-multiplexed configuration [16] to provide more focal planes.

In conclusion, we propose a polarization-multiplexed multiplane display design to overcome the VAC issue in HMD. The proposed design utilizes a polarization-sensitive bifocal Pancharatnam–Berry lens and a SPM to generate two independent focal image planes simultaneously. The proposed multiplane display requires no additional time-multiplexing operation, which can effectively reduce the display refresh rate by one half.

Funding. Intel Corporation.

REFERENCES

1. O. Cakmakci and J. P. Rolland, J. Disp. Technol. **2**, 199 (2006).
2. J. Geng, Adv. Opt. Photon. **5**, 456 (2013).
3. G. Kramida, IEEE Trans. Vis. Comput. Graph. **22**, 1912 (2016).
4. D. M. Hoffman, A. R. Girshick, K. Akeley, and M. S. Banks, J. Vis. **8**(3), 33 (2008).
5. M. Lambooij, M. Fortuin, I. Heynderickx, and W. IJsselsteijn, J. Imaging Sci. Technol. **53**, 030201 (2009).
6. J. P. Rolland, M. W. Krueger, and A. Goon, Appl. Opt. **39**, 3209 (2000).
7. G. Wetzstein, D. Lanman, W. Heidrich, and R. Raskar, ACM Trans. Graph. **31**, 1 (2012).
8. S. Lee, C. Jang, S. Moon, J. Cho, and B. Lee, ACM Trans. Graph. **35**, 60 (2016).
9. D. Lanman and D. Luebke, ACM Trans. Graph. **32**, 220 (2013).
10. B. T. Schowengerdt, R. S. Johnston, C. D. Melville, and E. J. Seibel, SID Symp. Dig. Tech. Pap. **43**, 640 (2012).
11. X. Hu and H. Hua, Opt. Express **22**, 13896 (2014).
12. S. Suyama, M. Date, and H. Takada, Jpn. J. Appl. Phys. **39**, 480 (2000).
13. S. Liu and H. Hua, Opt. Lett. **34**, 1642 (2009).
14. G. D. Love, D. M. Hoffman, P. J. W. Hands, J. Gao, A. K. Kirby, and M. S. Banks, Opt. Express **17**, 15716 (2009).
15. Y. H. Lee, G. Tan, T. Zhan, Y. Weng, G. Liu, F. Gou, F. Peng, N. V. Tabiryan, S. Gauza, and S. T. Wu, Opt. Data Process. Storage **3**, 79 (2017).
16. T. Zhan, Y. H. Lee, and S. T. Wu, Opt. Express **26**, 4863 (2018).
17. S. Liu, Y. Li, P. Zhou, Q. Chen, and Y. Su, Opt. Express **26**, 3394 (2018).
18. S. Pancharatnam, Proc. Indian Acad. Sci. Sect. A **44**, 247 (1956).
19. M. V. Berry, Proc. R. Soc. London Ser. A **392**, 45 (1984).
20. E. Hasman, V. Kleiner, G. Biener, and A. Niv, Appl. Phys. Lett. **82**, 328 (2003).
21. M. Schadt and W. Helfrich, Appl. Phys. Lett. **18**, 127 (1971).
22. J. Kim, Y. Li, M. N. Miskiewicz, C. Oh, M. W. Kudenov, and M. J. Escuti, Optica **2**, 958 (2015).
23. S. Lee, J. Cho, B. Lee, Y. Jo, C. Jang, D. Kim, and B. Lee, IEEE Access **6**, 2170 (2018).
24. R. Narain, R. A. Albert, A. Bulbul, G. J. Ward, M. S. Banks, and J. F. O'Brien, ACM Trans. Graph. **34**, 59 (2015).
25. K. Gao, C. McGinty, H. Payson, S. Berry, J. Vornehm, V. Finnemeyer, B. Roberts, and P. Bos, Opt. Express **25**, 6283 (2017).
26. C. Oh and M. J. Escuti, Opt. Lett. **33**, 2287 (2008).
27. G. Tan, Y. H. Lee, T. Zhan, J. Yang, S. Liu, D. F. Zhao, and S. T. Wu, Opt. Express **26**, 25076 (2018).
28. K. Akeley, S. J. Watt, A. R. Girshick, and M. S. Banks, ACM Trans. Graph. **23**, 804 (2004).
29. S. Liu and H. Hua, Opt. Express **18**, 11562 (2010).
30. K. J. MacKenzie, D. M. Hoffman, and S. J. Watt, J. Vis. **10**(8), 22 (2010).